Journal of Power Sources 215 (2012) 188–198

Contents lists available at SciVerse ScienceDirect

Journal of Power Sources

journal homepage: www.elsevier.com/locate/jpowsour

Quaternary PtMnCuX/C (X = Fe, Co, Ni, and Sn) and PtMnMoX/C (X = Fe, Co, Ni, Cu and Sn) alloys catalysts: Synthesis, characterization and activity towards ethanol electrooxidation

Malika Ammam, E. Bradley Easton*

Faculty of Science, University of Ontario Institute of Technology, 2000 Simcoe Street North, Oshawa, ON, Canada L1H 7K4

HIGHLIGHTS

- ► PtMnCuX/C (X = Fe, Co, Ni, and Sn) alloys have been synthetized and characterized.
- ► PtMnMoX/C (X = Fe, Co, Ni, Cu and Sn) alloys have been synthesized and characterized.
- ► All quaternary alloys showed superior activity towards ethanol oxidation.
- ► All quaternary alloys illustrated a facilitated oxidation of ethanol.

ARTICLE INFO

Article history:
Received 9 March 2012
Received in revised form
4 May 2012
Accepted 5 May 2012
Available online 12 May 2012

Keywords:
Ethanol oxidation
Electrocatalysis
Quaternary alloys PtMnCuX/C
(X = Fe, Co, Ni, and Sn) and PtMnMoX/C
(X = Fe, Co, Ni, Cu and Sn)

ABSTRACT

In this account, two series of quaternary PtMnCuX/C (X = Fe, Co, Ni, and Sn) and PtMnMoX/C (X = Fe, Co, Ni, Cu and Sn) alloys catalysts have been synthesized and characterized by ICP, XRD, XPS, TEM and cyclic voltammetry. XRD spectra of each series illustrated that PtMnCuX/C (X = Fe, Co and Ni) and PtMnMoX/C (X = Fe, Co, Ni and Cu) alloys have been formed without significant free Mn, Cu, Mo or X co-catalysts. For PtMnCuSn/C and PtMnMoSn/C, in addition to alloy formation, significant free Sn-oxides are present in each catalyst. Cyclic voltammetry and chronoamperometry revealed that all quaternary showed superior electrocatalytic activity towards ethanol oxidation compared to the ternary precursor. Also, shift of the onset potential of ethanol oxidation towards less positive values were also recorded with the quaternary alloys, demonstrating a facilitated oxidation with the quaternary alloys compared to ternary alloy precursor. The magnitude of the gain in potential depend on the alloy composition and PtMnMoSn/C was found to be the best of all synthetized quaternary alloys with an onset potential of ethanol oxidation of only 0.059 V vs. Ag/AgCl.

1. Introduction

The advantages of using fuel cells for the production of electricity in clean, silent and efficient way have been demonstrated [1–4]. Direct ethanol fuel cells (DEFCs) are considered among the most promising power devices because of their numerous advantages including less complex fuel storage systems compared to hydrogen fuel cells, low operating temperatures and easy handling. Furthermore, ethanol fuel with a high energy density and low toxicity can directly be produced from the fermentation of biomass.

Although DEFCs are good alternative power sources, their performance needs to be improved in order to make them suitable for many applications [5–7]. Carbon supported platinum (Pt) is commonly used as a catalyst in low temperature fuel cells. However, pure Pt is not an efficient anodic catalyst for DEFCs because Pt is well known to rapidly become poisoned on its surface by strongly adsorbed species such as CO that are formed by the initial dehydrogenation of the alcohol molecules, hence leading to substantial losses in operation potentials [8,9]. Due to the low electrocatalytic activity of pure Pt for practical DEFCs, elements such as Ru, Sn, Pd, W, Sn, Cu and Au have been added to form binary and ternary alloys to promote the electroactivity towards ethanol oxidation [10–21]. Furthermore, recent reports suggested that incorporation of a fourth metal to form quaternary alloys electrocatalysts such as PtRuMoW [22], PtRuCoW [23] and NiZrPtRu [24] can further increase the activity towards alcohol oxidation.

* Corresponding author. Tel.: +1 905 721 8668x2936; fax: +1 905 721 3304.
E-mail addresses: m78ammam@yahoo.fr (M. Ammam), Brad.Easton@uoit.ca (E.B. Easton).

0378-7753/$ – see front matter © 2012 Elsevier B.V. All rights reserved.
doi:10.1016/j.jpowsour.2012.05.007

Although the reasons for enhanced activity with Pt-alloy catalysts for alcohol oxidation are not yet fully understood, several studies suggest that is generally due to the ability of the promoter metal to generate the oxygenated species necessary for the complete oxidation of the alcohol at lower potentials [25]. On the other hand, removal of poisoning species adsorbed onto the catalyst surface has also been pointed out to be part of the mechanism [25]. Furthermore, the electronic effects have also been attributed to the presence of the other metal which weakens the bond between the poisoning species and the catalyst surface [26].

We have recently reported the synthesis, characterization and the catalytic activity of binary PtMn/C and ternary PtMnX/C (X = Fe, Co, Ni, Cu, Mo and, Sn) alloys catalysts and found that compared to Pt/C and PtMn/C, overall the ternary alloys catalysts exhibited higher catalytic activities towards ethanol oxidation [27,28]. The two best ternary alloys we identified were PtMnCu/C and PtMnMo/C, which illustrated the highest catalytic activity towards ethanol oxidation in terms of catalytic current and onset potential. In this study, based on these best ternary alloys, we have synthesized two series of quaternary alloys PtMnCuX/C (X = Fe, Co, Ni, and Sn) and PtMnMoX/C (X = Fe, Co, Ni, Cu and Sn). These new alloys have been characterized by ICP, XRD, XPS, TEM and cyclic voltammetry. Their catalytic activities towards ethanol oxidation were determined and compared to the catalysts precursors Pt/C, PtMn/C and ternary PtMnCu/C and PtMnMo/C.

2. Experimental

2.1. Materials

PtMn(19:81)/C, PtMnCu(17:43:40)/C and PtMnMo(17:61:22) were synthetized as previously reported [27,28]. For PtMn(19;81)/C, $H_2PtCl_6.6H_2O$ (Aldrich) and $MnCl_2.2H_2O$ (Aldrich) at the ratio of (23:77) were mixed in ultrapure water (milliQ, 18.2 MΩcm). After 15 min of constant stirring Vulcan XC72R carbon black (Cabot) was added to the solution in an amount to give a total metal content of 20 wt%. PtMn nanoparticles supported on carbon were formed by reduction of the metal precursors with $NaBH_4$, which was added as a solid to the mixture in a weight ratio of 3:1 to metals. The resulting mixture was then left under constant stirring over night and the formed supported catalysts were collected via suction filtration, washed thoroughly with ultrapure water, ethanol and acetone and finally dried over night at 80 °C. The ternary alloy catalysts PtMnCu(17:43:40)/C and PtMnMo/C(17:61:22)/C were synthesized by using the same procedure by replacing 20% (w/w) of $MnCl_2.2H_2O$ (Aldrich) by respectively $CuCl_2.2H_2O$ (Sigma–Aldrich) and $(NH_4)_2MoO_4$ (Aldrich) as previously reported [28]. The quaternary alloys were also formed following the same procedure by replacing 10% (w/w) of $CuCl_2.2H_2O$ (Sigma–Aldrich)in PtMnCu/C by $FeCl_3.6H_2O$ (Gelest Inc.), $Co(NO_3)_2.6H_2O$ (Sigma–Aldrich), $NiCl_2$ (Fluka), or $SnCl_2$ (Aldrich) and, 10% (w/w) of $(NH_4)_2MoO_4$ in PtMnMo/C by $FeCl_3.6H_2O$ (Gelest Inc.), $Co(NO_3)_2.6H_2O$ (Sigma–Aldrich), $NiCl_2$ (Fluka), $CuCl_2.2H_2O$ (Sigma–Aldrich) or $SnCl_2$ (Aldrich).

2.2. Materials characterization

Inductively Coupled Plasma Optical Emission Spectrometry (ICP-OES) was utilized for quantitative determination of metal content in the catalysts. 5 mg of each catalyst was dissolved in nitric acid (>70%) and left to dissolve for at least 1 week. Afterwards, the solutions were filtered off in order to separate the supporting carbon from the solution and yield a clear solution for ICP-OES analyses. Standardization was performed with three Pt, Mn, Fe, Co, Ni, Cu, Mo, and, Sn solutions ranging from approximately 1–20 ppm. These standards contained approximately 2% nitric acid to ensure the complete dissolution and keep both sample and standard matrices equivalent.

Energy Dispersive X-ray Spectroscopy (EDX) was used for a rapid, non-destructive determination of catalyst composition. EDX spectra were acquired using a JEOL JSM-7000F field emission scanning electron microscope equipped with an Oxford Systems INCA X-ray microanalyser.

Power X-ray diffraction (XRD) patterns were obtained using Bruker D8 Advance powder X-ray diffractometer, with germanium monochromator, Cu $K_{\alpha 1}$ radiation. The average grain size was determined from the broadening of the Pt(111) peak using the Scherrer equation.

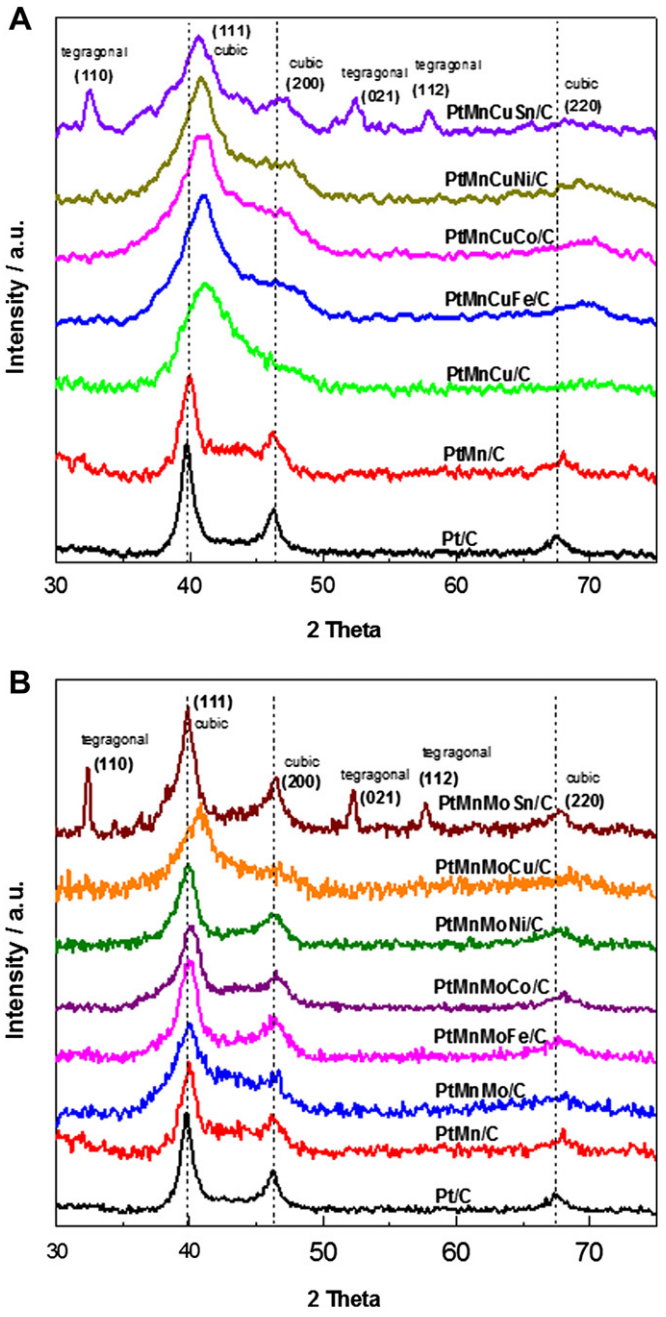

Fig. 1. X-ray diffractograms of Pt/C, PtMn/C and ternary alloys PtMnCu/C and PtMnMo/C and their corresponding series of quaternary alloys PtMnCuX/C (X = Fe, Co, Ni, and Sn) and PtMnMoX/C (X = Fe, Co, Ni, Cu and Sn) catalysts.

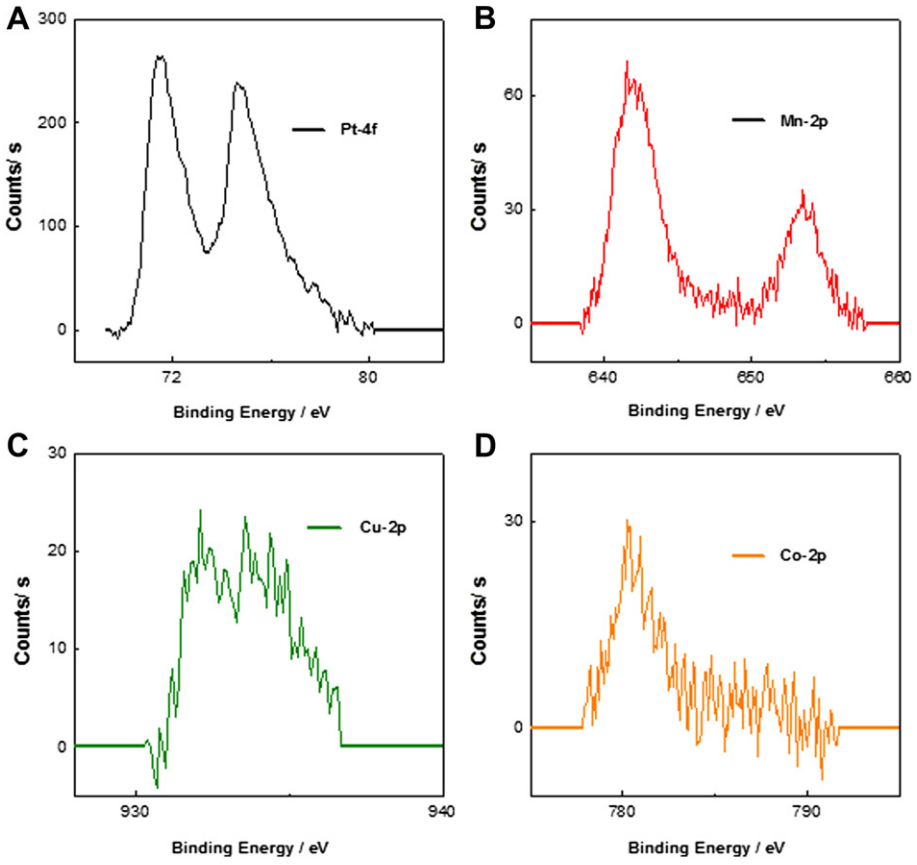

Fig. 2. XPS of Pt-4f (A), Mn-2p (B), Cu-2p (C) and Co-2p (D) of PtMnCuCo/C catalyst.

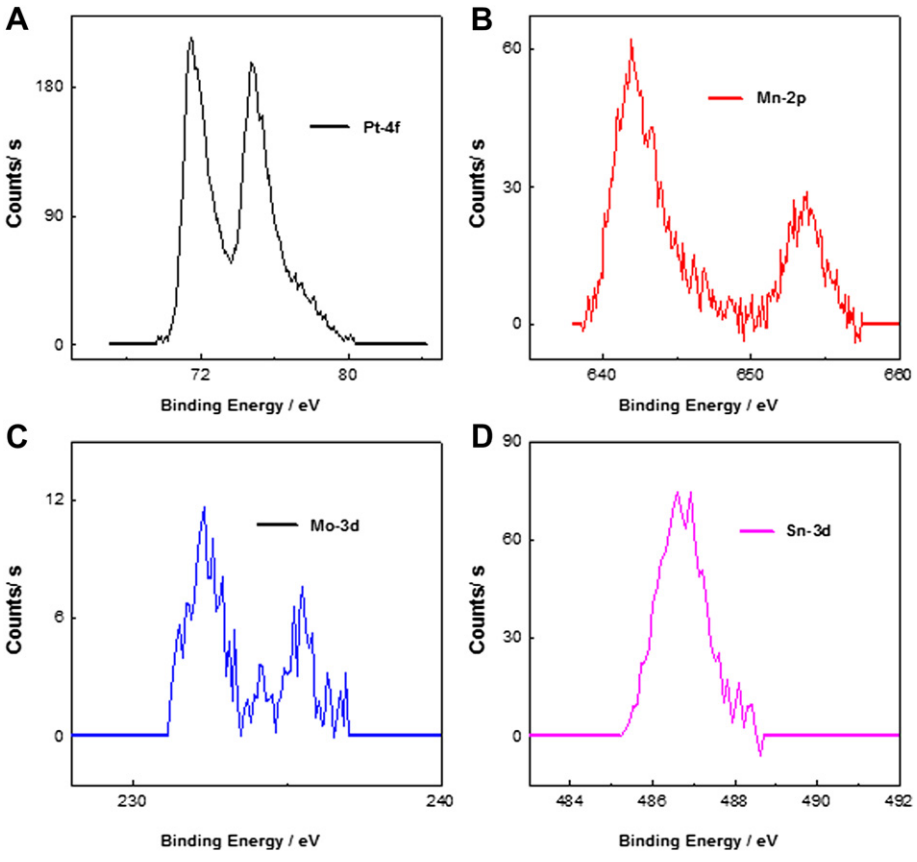

Fig. 3. XPS of Pt-4f (A), Mn-2p (B), Mo-3d (C) and Sn-3d (D) of PtMnMoSn/C catalyst.

X-ray photoelectron spectroscopy (XPS) was carried out using a Kratos Axis Ultra X-ray photoelectron spectrometer. Samples were dispersed in a mixture of ethanol and ultrapure water (50:50), deposited on silicon wafer supports and oven dried then analyzed.

Transmission Electron Microscopy (TEM) images were acquired using a Philips CM 10 instrument equipped with an AMT digital camera system. The catalysts powders were dispersed in ultrapure water and applied to nickel 400 mesh formvar coated carbon reinforced grids and allowed to dry under air. Grids were then scanned in a Philips CM 10 TEM at 100 kV.

2.3. Electrochemical characterization

The electrocatalytic activity of the catalysts towards ethanol oxidation was measured through the preparation of electrode inks, which were prepared as follows: 11 mg of the synthesized electrocatalyst was dispersed in 500 μL of a mixture of ultrapure water and 2-propanol (1:1 by volume) and the suspension was stirred in an ultrasonic bath for 15 min. 5 μL of the catalysts ink was immobilized onto the surface of a glassy carbon (GC) electrode (daim. = 3 mm, CH Instruments) and dried at 80 °C for 20 min. Afterwards, 5 μL Nafion (5% in alcohols, Ion Power) was deposited on top of each surface and dried again in the oven at 80 °C for 10 min. The Nafion deposition layer prevents the catalyst deposited layer from peeling of the GC electrode. Prior to use, the GC electrodes were first polished with 6, 3 and 1 μm alumina then abundantly rinsed with ultrapure water and acetone. The final loading of metal catalysts on each electrode was 0.30 ± 0.03 mg cm^{-2}.

All electrochemical measurements were performed using a Solartron SI 1286 potentiostat controlled using Corrware software (Scribner Associates). A three-compartment electrochemical cell was used. The side arms contained a Ag/AgCl reference electrode and a platinum counter electrode. Measurements were made at room temperature using either N_2-purged 0.5 M H_2SO_4 (aq) or N_2-purged 0.5 M H_2SO_4 containing 0.17 M ethanol.

Some of the electrochemical data were normalized to the electrochemical active surface area of Pt (in cm^2) that is determined from the charge density q_{Pt} (C cm^{-2} electrode) obtained from the cyclic voltammetry experiment of Fig. 4 divided on the charge required to reduce a monolayer of protons on Pt($\Gamma = 210\mu C/cm^2_{Pt}$).

$$ECSA(cm^2_{Pt}) = q_{Pt}/\Gamma$$

3. Results and discussion

3.1. Materials characterization

3.1.1. ICP analyses

Table 1 gathers the calculated molar ratios used for the synthesis of the two series of quaternary alloys with respect to ternary, binary and Pt/C precursors and the corresponding atomic ratios determined by ICP as well as the average grain size of each catalyst estimated from the XRD measurements. For both quaternary alloys catalysts PtMnCuX/C (X = Fe, Co, Ni, and Sn) and PtMnMoX/C (X = Fe, Co, Ni, Cu and Sn), a difference between the calculated values used during the synthesis and the determined values using ICP can be noticed and this difference is overall more pronounced for quaternary catalysts based Mo than Cu. The latter has to be expected since during the reaction with $NaBH_4$, the mixed metal cations (Pt^{4+}, Mn^{2+} and X^{n+}) can partially or entirely react during the reduction process to form the alloyed nanoparticles. The latter depends on several parameters including the concentration of the reactants (metal cations and reducing agent), nature of the reactants (metal cations), the reaction conditions such as temperature, pH, hydrodynamic agitation and more importantly of the ionization energy or potential of the metal cations [29,30]. The latter may influence the kinetics of the reduction reaction and formation of the alloyed nanoparticles. Similar differences between the utilized and the determined ratios of the metal co-catalysts have also been noticed in literature [31,33]. EDX was performed on some of the catalysts revealed similar values as those determined by ICP. Also that carbon is the dominant element in the composition with about 80% by weight, which confirms the amount of the experimentally employed carbon during the synthesis of the catalysts.

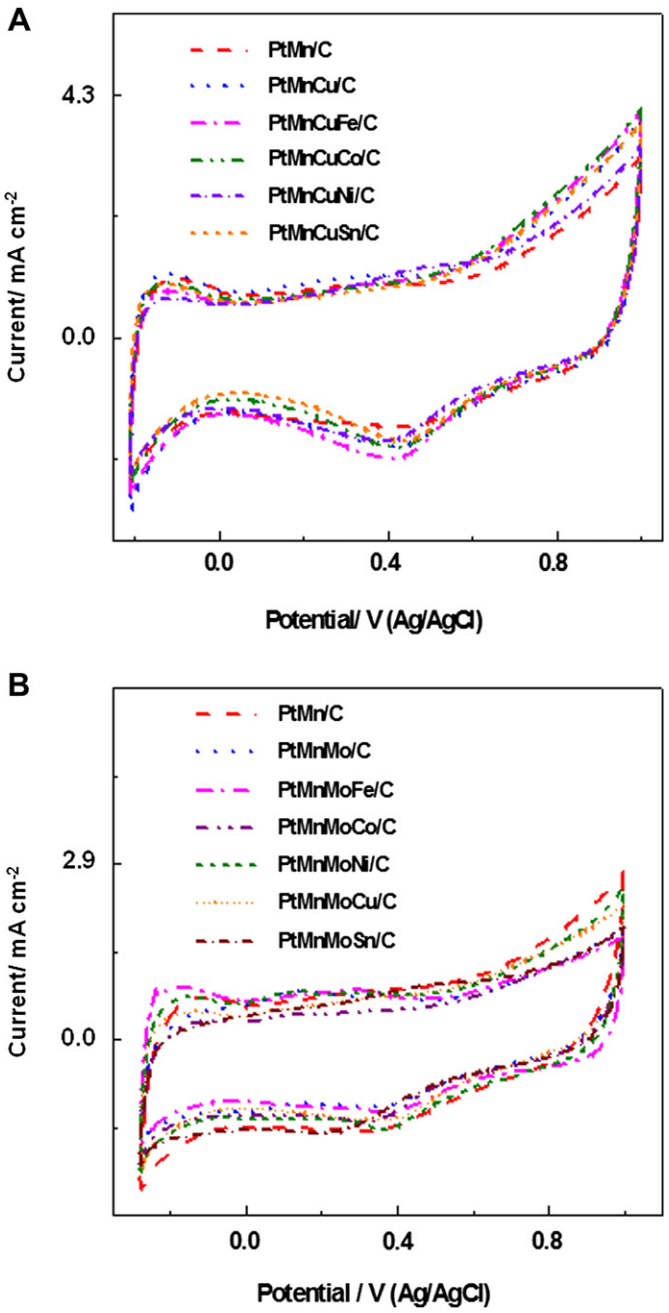

Fig. 4. Cyclic voltammetry curves in 0.5 M H_2SO_4 at 20 mV s^{-1} of PtMn/C, PtMnCu/C and PtMnCuX/C (X = Fe, Co, Ni, and Sn) (A) and PtMnMoX/C (X = Fe, Co, Ni, Cu and Sn) catalysts (B).

Table 1
Calculated molar ratios and measured atomic ratios by ICP of the synthesized Pt/C, PtMn/C, PtMnCu/C, PtMnMo/C and quaternary alloys PtMnCuX/C (X = Fe, Co, Ni, and Sn) and PtMnMoX/C (X = Fe, Co, Ni, Cu and Sn). Also is shown the average grain size calculated from X-ray diffraction data using the Debye–Scherrer equation.

Electrocatalysts	Molar ratios used for the synthesis				Molar ratios measured by ICP				Molar ratios measured by XPS				Grain size (nm ± 0.5)	
	Pt	**Mn**	**-**	**-**	**Pt**	**Mn**	**-**	**-**	**Pt**	**Mn**	-	-	**Cubic**	**Tetragonal**
Pt/C	100	0	-	-	100	0	-	-	100	0	-	-	8.5	-
PtMn/C	23	77	-	-	19	81	-	-	19	81	-	-	7.5	-
	Pt	**Mn**	**Cu**	**X**	**Pt**	**Mn**	**Cu**	**X**	**Pt**	**Mn**	**Cu**	**X**	**Cubic**	**Tetragonal**
PtMnCu/C	24	50	26	-	17	43	40		-	-	-	-	3.5	-
PtMnCuFe/C	26	50	16	8	31	40	18	11	20	53	13	14	3.1	-
PtMnCuCo/C	25	51	16	8	17	46	24	13	17	66	8	9	4.0	-
PtMnCuNi/C	23	47	15	15	26	42	20	12	-	-	-	-	4.0	-
PtMnCuSn/C	24	49	15	12	24	30	12	34	25	50	12	13	5.0	17.0
	Pt	**Mn**	**Mo**	**X**	**Pt**	**Mn**	**Mo**	**X**	**Pt**	**Mn**	**Mo**	**X**	**Cubic**	**Tetragonal**
PtMnMo/C	25	53	22	-	17	61	22	-	-	-	-	-	4.5	-
PtMnMoFe/C	26	52	13	9	21	41	24	14	-	-	-	-	6.0	-
PtMnMoCo/C	26	53	13	8	12	67	4	17	17	70	4	9	6.0	-
PtMnMoNi/C	22	45	12	21	30	48	6	16	20	69	2	9	6.0	-
PtMnMoCu/C	24	48	12	16	31	50	4	15	-	-	-	-	4.5	-
PtMnMoSn/C	25	51	13	11	14	37	3	46	27	55	3	15	6.0	26.0

3.1.2. X-ray diffraction pattern

Fig. 1 illustrates the X-ray diffractograms of the two synthetized series of quaternary alloys PtMnCuX/C (X = Fe, Co, Ni, and Sn) (Fig. 1A) and PtMnMoX/C (X = Fe, Co, Ni, Cu and Sn) (Fig. 1B) along with the respective ternary alloys precursors PtMnCu/C and PtMnMo/C as well as PtMn/C and Pt/C. It can be seen that Pt/C electrocatalyst displays three main Bragg peaks located at scattering angles of ca. 40°, 46° and 67°, which are characteristic of the fcc structure of platinum [19,21]. The diffractograms of the binary alloy PtMn/C display some changes in the form and shape of these peaks as previously discussed [27]. Incorporation of a third metal Cu or Mo in PtMn/C catalyst leads to a more pronounced change in the form and position of the Pt peaks [28]. Overall, the peaks become broader and display a shift towards higher angles. Addition of a fourth metal in PtMnCu/C and PtMnMo/C leads to further changes in the Pt main peaks. Moreover, Fig. 1 clearly displays that

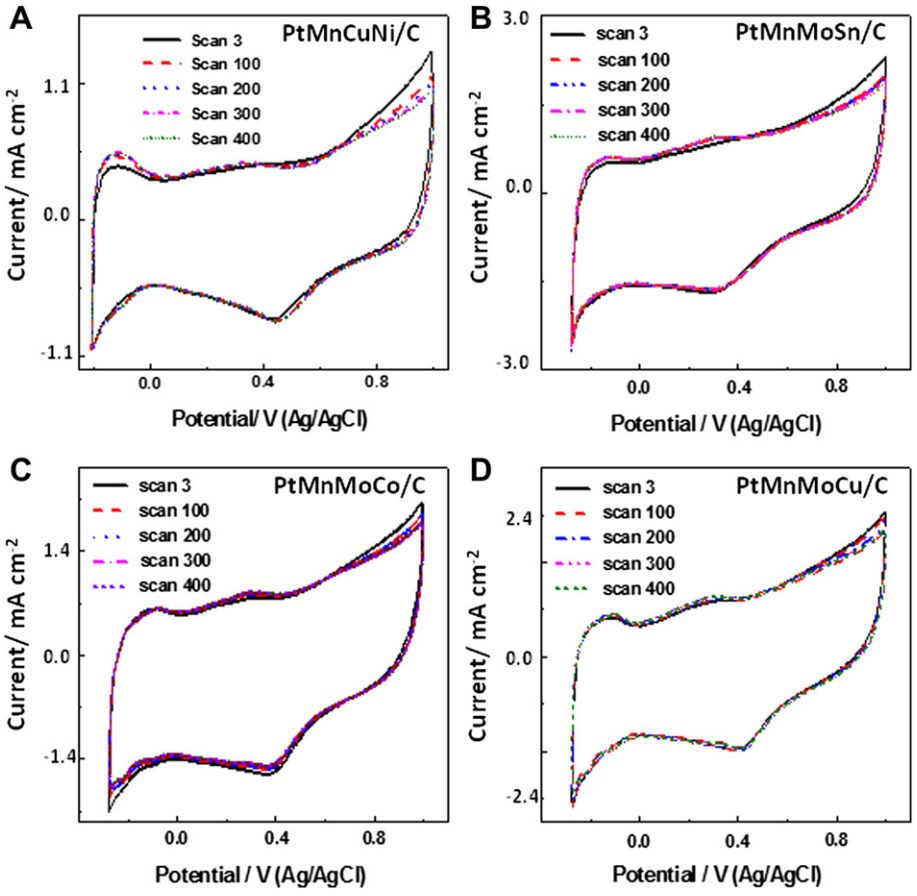

Fig. 5. Comparison between the 3rd, 100, 200, 300 and 400th cycle in 0.5 M H_2SO_4 at 50 mV s^{-1} of PtMnCuNi/C (A), PtMnMoSn/C (B), PtMnMoCo/C (C) and PtMnMoCu/C (D).

the changes in the three main peaks of Pt are more visible for Cu containing alloys. This may suggest that Cu based alloys contain some free Cu co-catalyst. However, according to literature, XRD spectra of Cu contain a large peak at scattering angle of 51° [34], which unlikely is absent in the Cu-based catalysts of Fig. 1. Therefore, the visible change in shape and position of the main Pt peaks observed with Cu-containing catalysts might be related to formation of alloys and since Cu-containing catalysts showed the smallest grain sizes (Table 1), this may in part explain the observed significant widening of the peaks, demonstrating the formation of alloys. The latter can further be confirmed by analyzing the XRD data shown in Table S1 of the supplementary information. It should be noted that incorporation of the co-catalysts in the Pt lattice overall decreases the *d* spacing. This is understandable because all the employed co-catalysts Mn, Cu, Mo, Fe, Co, Ni and Sn have smaller atomic sizes than that of Pt, thus their incorporations in the Pt lattice to form the alloys will lead to a decrease in the cell lattice or *d* spacing. On the other hand, while no particular significant new peaks appear at other angles for the two series of quaternary alloys based PtMnCuX/C (X = Fe, Co and Ni) (Fig. 1A) and PtMnMoX/C (X = Fe, Co, Ni and Cu), which indicate the absence of a high amount of free co-catalyst oxides [35,42], and demonstrating in part the incorporation of the metals co-catalysts into the Pt lattice to form intermetallic phases, both PtMnCuSn/C and PtMnMoSn/C display visible other peaks located between the main Pt peaks. This suggests that in addition to formation of the alloyed PtMnCuSn/C and PtMnMoSn/C nanoparticles, a significant amount of free Sn and Sn oxides such as SnO_2 and SnO are formed [43–45]. It is worth noting that similar observations were reported previously with the ternary alloy PtMnSn/C. These repetitive observations might be related to the synthetic method used in these studies. $NaBH_4$ is a strong reducing agent and under these conditions; the reduction of Sn into oxides is much more favorable compared to the other elements. The latter is reflected in the particles sizes shown in Table 1 where it can be seen that all the catalysts display one cubic phase assigned to fcc of Pt with an average grain size varying from 3–8 nm, PtMnCuSn/C and PtMnMoSn/C display an additional tetragonal phase with larger grain sizes of 17 nm and 26 nm, respectively. The latter could be assigned to SnO_2 and SnO oxides [43].

3.1.3. XPS characterization

In order to confirm the presence of all elements in the quaternary alloyed nanoparticles as well as possible electronic effects of the co-catalysts, some of the catalysts have been analyzed by XPS. Figs. 2 and 3 illustrate typical examples of XPS analysis of PtMnCuCo/C and PtMnMoSn/C, respectively. The presence of Pt, Mn, Mo and Sn in PtMnMoSn/C and Pt, Mn, Cu and Co in PtMnCuCo/C with significant intensities that is located at the appropriate binding energies of the co-catalysts, confirming that quaternary alloyed nanoparticles are formed. Furthermore, quantitative analyses of the XPS data revealed different compositions from that determined by ICP (Table 1). This indicates that the composition of the quaternary alloyed nanoparticles at the surface differs from the bulk. The latter might be explained by surface segregations of the alloyed nanoparticles, which in turn may affect the catalytic

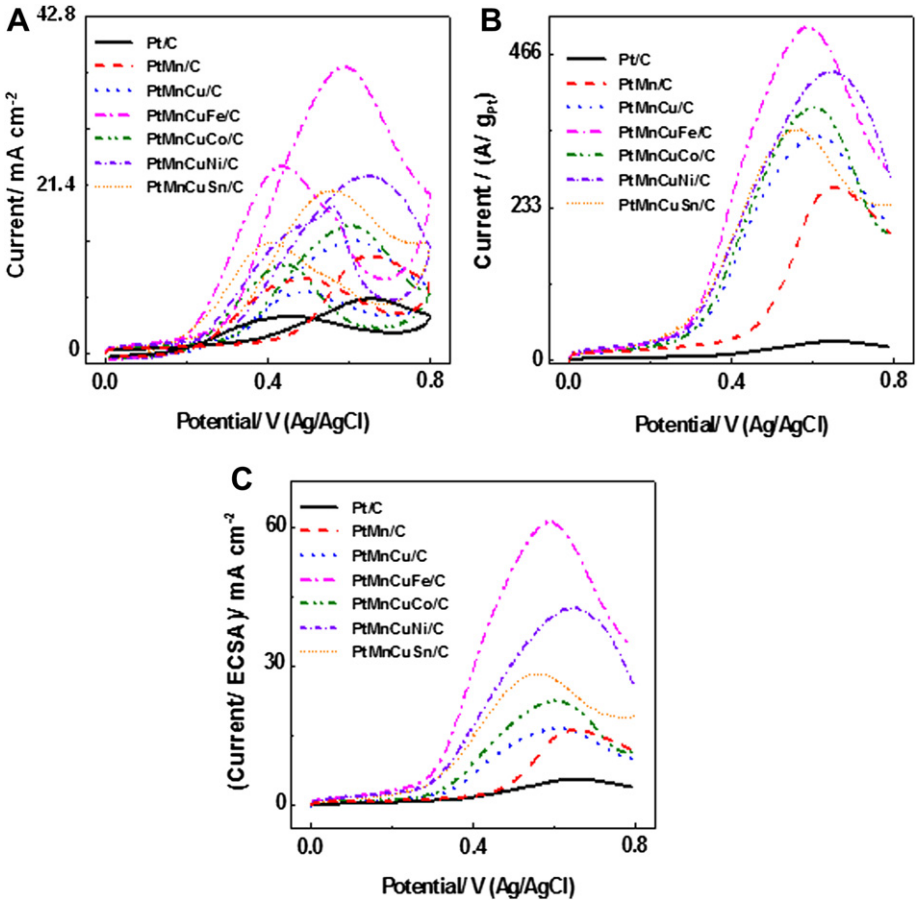

Fig. 6. (A) Cyclic voltammetry curves of Pt/C, PtMn/C, PtMnCu/C and PtMnCuX (X = Fe, Co, Ni, and Sn) alloys electrocatalysts in 0.5 M H_2SO_4 containing 0.17 M ethanol, (B) is (A) without reverse scan normalized per g of Pt and, (C) is (A) without reverse scan normalized by ECSA. Scan rate 20 mV s^{-1}.

properties of the alloys [27,28]. For example, while ICP analysis of PtMnMoSn/C point to a low bulk Pt content (14%); XPS reveals a high surface Pt content (27%). This indicates that PtMnMoSn/C nanoparticles are Pt rich at the surface. The latter may significantly affect the catalytic properties of PtMnMoSn/C.

3.1.4. Electrochemical characterization

Fig. 4 displays the cyclic voltammetry curves in 0.5 M H_2SO_4 obtained for two series of the synthesized quaternary alloys PtMnCuX/C (X = Fe, Co, Ni, and Sn) (Fig. 4A) and PtMnMoX/C (X = Fe, Co, Ni, Cu and Sn) (Fig. 4B). Also is shown the binary PtMn/C and the ternary alloys PtMnCu/C and PtMnMo/C precursors. While the PtMnCuX/C (X = Fe, Co, Ni, and Sn) catalysts series show more or less similar charge in the hydrogen adsorption region as well as in the oxide region (Fig. 4A), the cyclic voltammograms of the series of PtMnMoX/C (X = Fe, Co, Ni, Cu and Sn) catalysts illustrate more variations in these regions. This is consistent with the ICP data (Table 1), where more significant variations in the Pt amounts between the catalysts can be noticed for the Mo than Cu based quaternary alloys, which are also confirmed by XPS of some of the analyzed catalysts. The cyclic voltammograms of the two series of quaternary alloys catalysts were subjected to cycling is 0.5 H_2SO_4 for at least 400 cycles. Fig. 5 displays typical examples of how the cyclic voltammetry curves of some of the quaternary catalysts after repetitive cycles. Fig. 5A depicts a slight increase in the hydrogen adsorption region for PtMnCuNi/C after 200 cycles. This suggests an increase in the surface of Pt in PtMnCuNi/C after 200 cycles, which might be due a slight corrosion of the catalyst after cycling in sulfuric acid. This is not surprising since similar observations have been reported elsewhere for Pt alloys such as PtNi/C and PtCu/C [46–49]. On the other hand, it is found that the Mo based quaternary alloys overall show better stability compared to Cu based quaternary catalysts. As depicted especially in Fig. 5C and 5D for PtMnMoCo/C and PtMnMoCu/C, no significant change in the shape or form of the cyclic voltammograms can be noticed after 400 cycles. This indicates a minimal corrosion rate of these series of alloys in sulfuric acid despite their high content with non-Noble metals. The latter maybe related to presence of Mo, even in small amounts, in the catalysts which confers a better stability to the quaternary alloy.

4. Catalytic activity of the quaternary alloys PtMnCuX/C (X = Fe, Co, Ni, and Sn) and PtMnMoX/C (X = Fe, Co, Ni, Cu and Sn) towards ethanol oxidation

The activity of the two series of Cu and Mo based quaternary alloys catalysts towards ethanol oxidation with respect to ternary, binary and Pt/C is shown in Figs. 6A and 7A, respectively. It can be seen that for both series of quaternary alloys PtMnCuX/C (X = Fe, Co, Ni, and Sn) and PtMnMoX/C (X = Fe, Co, Ni, Cu and Sn), an increase in the electrocatalytic activity can be observed with respect to ternary alloys precursors PtMnCu/C and PtMnMo/C, respectively. Furthermore, contrary to the Sn based catalyst PtMnSn/C reported previously that showed a very moderate

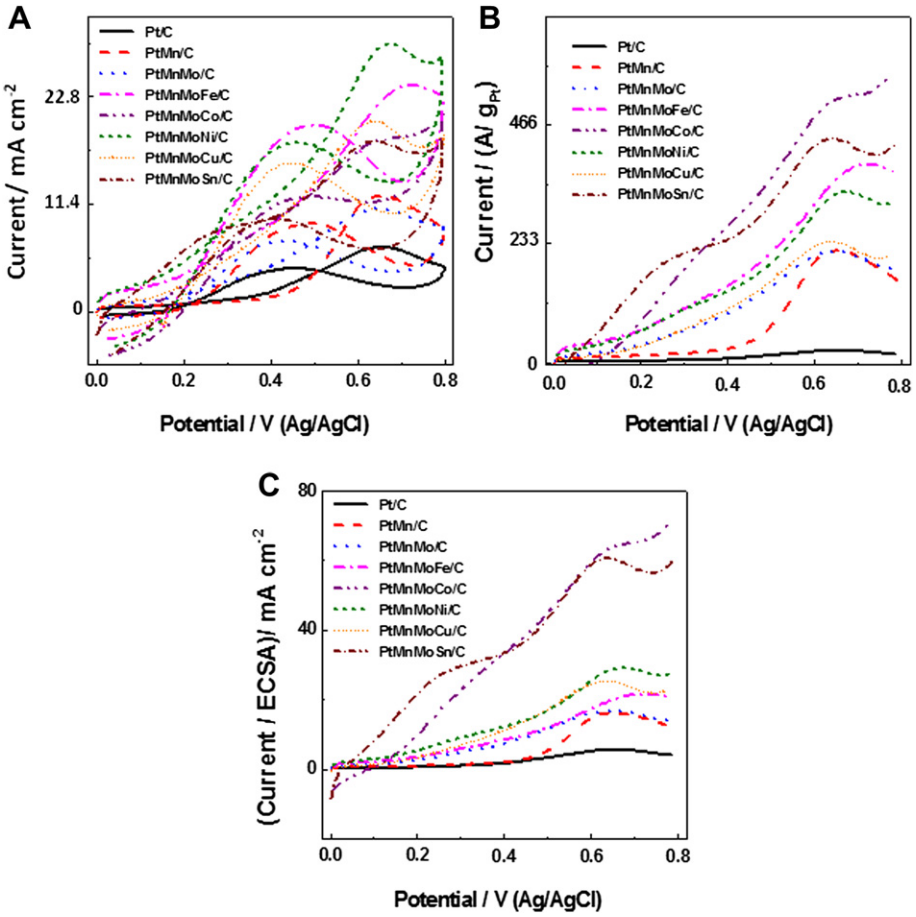

Fig. 7. (A) Cyclic voltammetry curves of Pt/C, PtMn/C, PtMnMo/C and PtMnMoX/C (X = Fe, Co, Ni, Cu and Sn) catalysts in 0.5 M H_2SO_4 containing 0.17 M ethanol, (B) is (A) without reverse scan normalized per g of Pt and, (C) is (A) without reverse scan normalized by ECSA. Scan rate 20 mV s^{-1}.

catalytic activity [28], Sn based quaternary alloys PtMnCuSn/C and PtMnMoSn/C seem to have high catalytic activities. The latter may have to do with the particle sizes as well as their distribution on the supporting carbon. Whereas agglomerations have been observed with PtMnSn/C [28], the TEM images shown in Fig. 8 for PtMnCuSn/C depict little agglomeration with well dispersed metal particles on the carbon support. With respect to grain sizes, it can be seen that most particles are small with some larger nanoparticles, which confirms to some extent the results of the grain size estimated by XRD (Table 1). This in turn confers to the alloy catalyst a better surface to volume ratio, thus a better catalytic activity.

Figs. 6B and 7B compares the ethanol oxidation activities of the two series of the quaternary alloys catalysts normalized to the amount of Pt present in each catalyst. The activities towards ethanol oxidation of the Cu and Mo based quaternary alloys catalysts normalized per g of Pt estimated at 0.5 V are listed in Table 2, with respect to the catalysts precursors Pt/C, PtMn/C and ternary PtMnCu/C and PtMnMo/C for each series. It can be noticed that all the alloy catalysts display higher catalytic activities than Pt/C and PtMn/C. Also, the relative activity of the quaternary alloys PtMnCuX/C (X = Fe, Co, Ni, and Sn) and PtMnMoX/C (X = Fe, Co, Ni, Cu and Sn) increased compared to the ternary alloys PtMnCu/C and PtMnMo/C. From Table 2, it can be seen that the catalytic activity increases in the following order: PtMnCuFe/C > PtMnCuNi/C > PtMnCuSn/C > PtMnCuCo/C for the Cu based quaternary alloys and PtMnMoCo/C > PtMnMoSn/C > PtMnMoFe/C > PtMnMoNi/C > PtMnMoCu/C for the Mo based quaternary catalysts. Table 2, also displays that compared to binary PtMn/C, the Cu based quaternary catalysts overall perform higher relative activities compared to Mo based quaternary catalysts. The nature of the co-catalyst present in the alloy as well as surface segregations properties would be the main reason for the observed enhanced catalytic activities [25,26]. Table 2 reveals that incorporation of a fourth metal in each ternary alloy PtMnCu/C and PtMnMo/C influences not

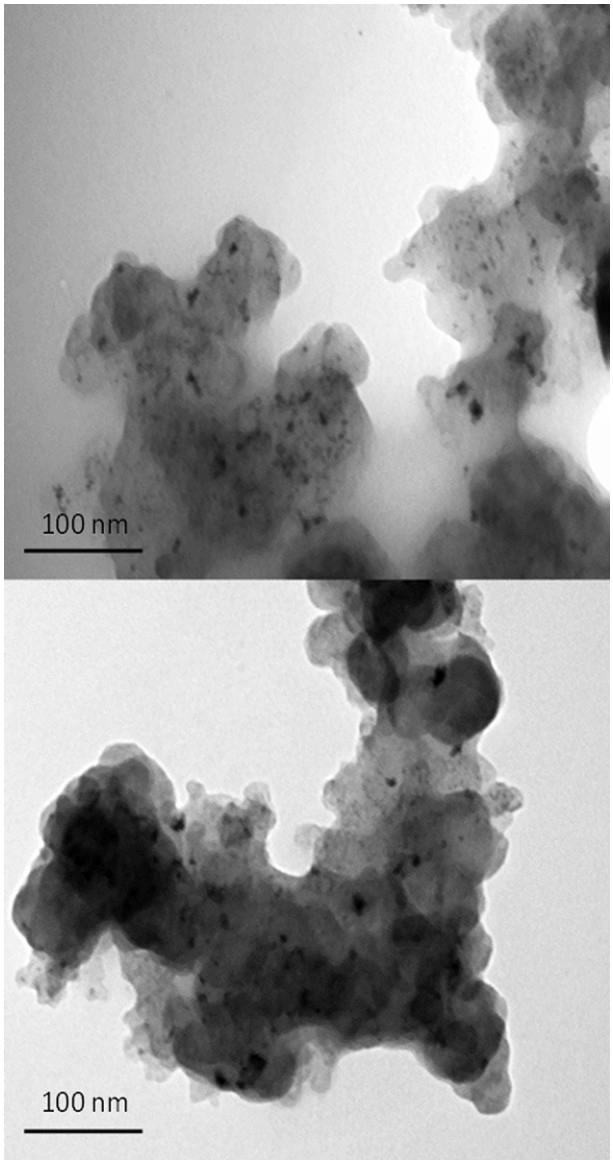

Fig. 8. TEM images of PtMnCuSn/C.

Table 2
Summary of the synthesized alloys and their normalized relative activities to pure Pt/C, binary PtMn/C, and ternary alloys PtMnCu/C and PtMnMo/C precursors for each series estimated at 0.5 V and the corresponding onset potential for ethanol oxidation (Data taken from Figs. 6B and 7B).

Synthesized catalyst	Normalized activity (A/g_{Pt})	Relative activity to pure Pt	Relative activity to PtMn/C	Relative activity to (PtMnCu/C)/(PtMnMo/C)	Onset potential
Pt/C	17.31	1	0.18	0.06	0.328
PtMn/C	91.45	5.28	1	0.32	0.402
Cu based catalysts					
PtMnCu/C	279.01	16.11	3.05	1	0.284
PtMnCuFe/C	432.09	24.96	4.72	1.54	0.236
PtMnCuCo/C	312.22	18.03	3.41	1.11	0.272
PtMnCuNi/C	326.2	18.84	3.56	1.16	0.232
PtMnCuSn/C	320.37	18.50	3.50	1.14	0.239
Mo based catalysts					
PtMnMo/C	145.62	8.41	1.59	1.00	0.227
PtMnMoFe/C	213.58	12.33	2.33	1.46	0.167
PtMnMoCo/C	357.26	20.63	3.09	2.45	0.142
PtMnMoNi/C	190.28	10.99	2.08	1.30	0.148
PtMnMoCu/C	159.21	9.19	1.74	1.09	0.224
PtMnMoSn/C	310.66	17.94	3.39	2.13	0.059

Table 3
Summary of the synthesized alloys and their normalized relative activities to pure Pt/C, binary PtMn/C, and ternary alloys PtMnCu/C and PtMnMo/C precursors for each series estimated at 0.5 V by taking into account ECSA (Data taken from Figs. 6C and 7C).

Synthesized catalyst	Normalized activity ($mA\ cm^{-2}$)	Relative activity to pure Pt	Relative activity to PtMn/C	Relative activity to (PtMnCu/C)/(PtMnMo/C)
Pt/C	3.3	1	0.62	0.24
PtMn/C	5.3	1.60	1	0.39
Cu based catalysts				
PtMnCu/C	13.3	4.03	2.50	1
PtMnCuFe/C	51.5	15.06	9.71	3.87
PtMnCuCo/C	18.0	5.45	3.39	1.35
PtMnCuNi/C	31.0	9.39	5.84	2.33
PtMnCuSn/C	26.3	7.96	4.96	1.97
Mo based catalysts				
PtMnMo/C	11.3	3.42	2.13	1.00
PtMnMoFe/C	12.1	3.66	2.28	1.07
PtMnMoCo/C	44.9	13.60	8.47	3.97
PtMnMoNi/C	17.0	5.15	3.20	1.50
PtMnMoCu/C	17.4	5.27	3.28	1.53
PtMnMoSn/C	43.4	13.15	8.18	3.84

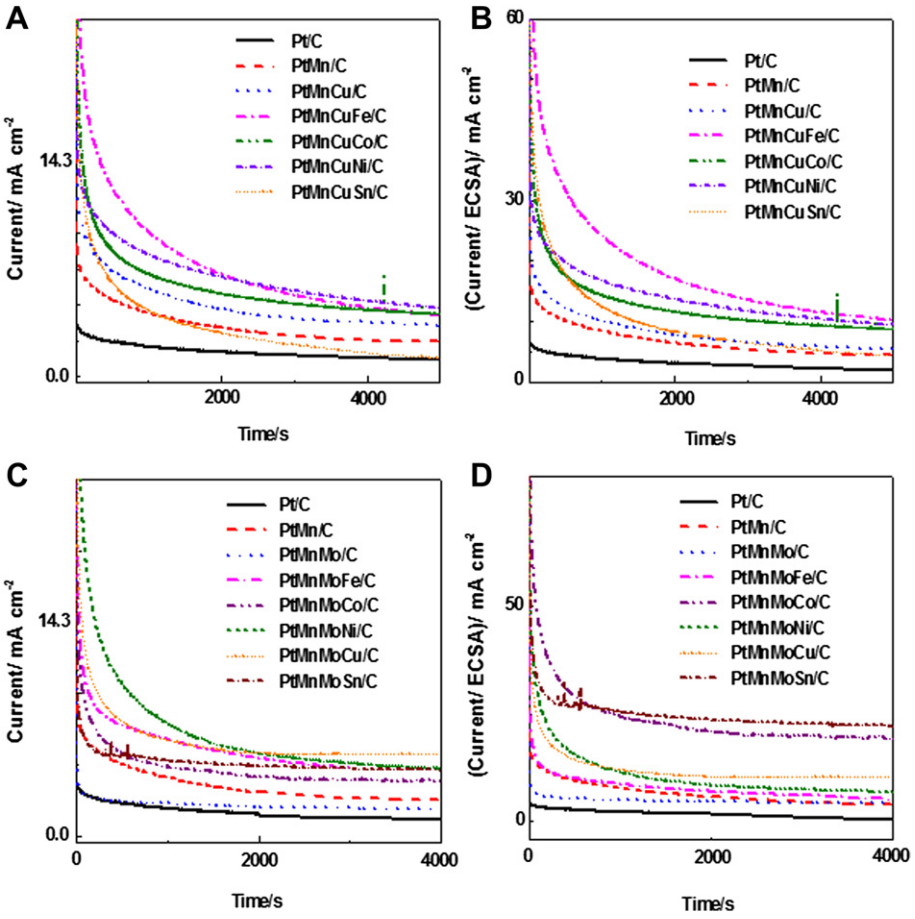

Fig. 9. (A) Current density time curves at +0.6 V in 0.5 M H_2SO_4 containing 0.17 M ethanol of Pt/C, PtMn/C and PtMnCu/C and PtMnCuX/C (X = Fe, Co, Ni and, Sn) and, (B) is (A) normalized by ECSA. (C) Current density time curves at +0.6 V in 0.5 M H_2SO_4 containing 0.17 M ethanol of Pt/C, PtMn/C, PtMnMo/C and PtMnMoX/C (X = Fe, Co, Ni, Cu and Sn) alloys catalysts and, (D) is (C) normalized by ECSA.

only the catalytic current efficiencies towards ethanol oxidation, but also the onset potentials. Table 2 depicts that compared to the ternary alloys precursors PtMnCu/C and PtMnMo/C, all the quaternary alloys display a shift in the onset potential towards less positive values. The magnitude of the shift depends on the alloy composition and the recorded gains in potentials are higher with Mo compared to Cu based quaternary alloys. Precisely, 60, 85, 79, 3 and 168 mV are the gains in potentials recorded with respectively PtMnMoFe/C, PtMnMoCo/C, PtMnMoNi/C, PtMnMoCu/C and PtMnMoSn/C versus 48, 12, 52 and 45 mV for PtMnCuFe/C, PtMnCuCo/C, PMnCuNi/C and PtMnCuSn/C, respectively. This means that ethanol electrooxidation is facilitated and needs less overpotentials with the quaternary alloys with respect to the ternary alloy precursors PtMnCu/C and PtMnMo/C, respectively. The latter may be related to modification of the electronic structures of the new catalysts, which facilitate C–C bond breaking and hence a better ethanol oxidation [50].

Figs. 6C and 7C are Figs. 6A and 7A normalized to the ECSA of each catalyst. The catalytic efficiencies of the catalysts towards ethanol oxidation normalized to ECSA are gathered in Table. 3. Overall, by taking ECSA into consideration, the quaternary alloys still depict higher catalytic efficiencies compared to the ternary precursors.

The superior performance of the quaternary alloys with respect to the ternary, binary and Pt/C precursors are also reflected in the chronoamperometry measurements shown in Fig. 9A and C for respectively for Cu and Mo based quaternary alloys. Fig. 9B and D are Fig. 9A and C normalized to the ECSA. In all current-time curves there is an initial current drop during the first 500 s followed by a relatively slower decay, but the currents obtained with the quaternary alloys of both Cu and Mo based series are overall higher than those obtained with the ternary alloys, binary PtMn/C and Pt/C consistent with the results of Figs. 6 and 7. Fig. 9 also reveals that overall Mo based quaternary alloys show better stability in 0.5 M H_2SO_4 containing 0.17 M ethanol compared to Cu based quaternary alloys because stabilization of the current occurs more quickly and last for long period of time. However, the currents obtained with Mo based catalysts are overall lower than those obtained with Cu based quaternary series consistent also with the results of cyclic voltammetry of Figs. 6 and 7. The stability of the alloys in sulfuric acid and in presence of ethanol was further tested by cyclic voltammetry and typical examples are shown in Fig. 10. A decrease in the current intensities can be noticed after 200 cycles for PtMnCuCo/C and PtMnMoCu/C. The latter might be related either to corrosion of the catalysts after 200 cycles or simply to a decrease in the concentration of ethanol because of its continuous oxidation during 200 cycles. On the other hand, Fig. 10C depicts that even with pure Pt/C, similar reductions in the current intensities are obtained after 200 cycles. Therefore, we conclude that stability of the quaternary alloys are comparable to that of Pt/C, of which the degradation mechanisms are well known to some extent [40].

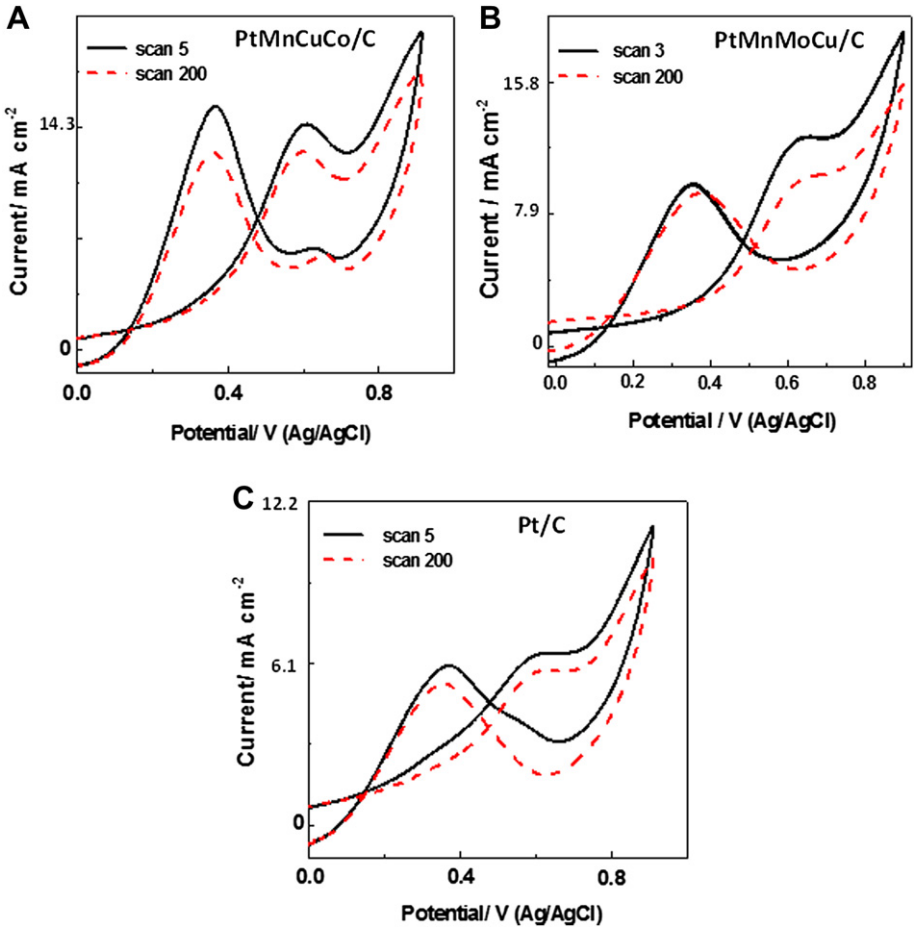

Fig. 10. Cyclic voltammograms of PtMnCuCo/C (A), PtMnMoCu/C (B) and Pt/C (C) over 200 cycles in 0.5 M H_2SO_4 containing 0.17 M ethanol.

5. Conclusions

Two series of quaternary alloys PtMnCuX/C (X = Fe, Co, Ni, and Sn) and PtMnMoX/C (X = Fe, Co, Ni, Cu and Sn) have been synthesized and characterized by ICP, XRD, XPS, TEM and cyclic voltammetry. XRD spectra of each series illustrated that PtMnCuX/C (X = Fe, Co and Ni) and PtMnMoX/C (X = Fe, Co, Ni and Cu) alloys have been formed without significant free Mn, Cu, Mo or X co-catalysts. For PtMnCuSn/C and PtMnMoSn/C, in addition to alloy formation, significant free Sn-oxides are present in each catalyst. Cyclic voltammetry and chronoamperometry revealed that all quaternary alloys showed superior electrocatalytic activity towards ethanol oxidation compared to the ternary precursor. A shift of the onset potential of ethanol electrooxidation towards less positive values were also recorded with the quaternary alloys, demonstrating a facilitated oxidation with the quaternary alloys compared to ternary alloy precursor. The magnitude of the gain in potential depends on the alloy composition. PtMnMoSn/C was found to be the best of all synthesized quaternary alloys with an onset potential of ethanol oxidation of only 0.059 V vs. Ag/AgCl. Overall, incorporation of a fourth metal in the ternary PtMnCu/C and PtMnMo/C leads to quaternary alloys with better catalytic activity towards ethanol oxidation.

Acknowledgement

This work was supported by Alcohol Countermeasure Systems Corp., the Natural Sciences and Engineering Research Council (NSERC) of Canada and UOIT. We thank Andrew Pedersen (UOIT) and Steve Koprich (McMaster University) for the EDX analyses, Wen He Gong (McMaster University) for the XRD data, Michael Allison (UOIT) for assistance with the ICP measurements, Dr. Richard B. Gardiner (University of Western Ontario) for the TEM images and Mark C. Biesinger (University of Western Ontatio) for the XPS data.

Appendix A. Supplementary information

Supplementary information associated with this article can be found, in the online version, at doi:10.1016/j.jpowsour.2012.05.007

References

[1] S. Srinivasan, R. Mosdale, P. Stevens, C. Yang, Annual Review of Energy and the Environment 24 (1999) 281–328.
[2] M.W. Ellis, M.R. Von Spakovsky, D.J. Nelson, Proceedings of the IEEE 89 (2001) 1808–1818.
[3] W. Vielstich, A. Lamm, H.A. Gasteiger, Handbook of Fuel Cells: Fundamental, Technology, and Applications, Wiley, Chichester, U.K. and Hoboken, NJ, 2003.
[4] S. Srinivasan, Fuel Cells: From Fundamentals to Applications, Springer, New York, 2006.
[5] W. Qian, D.P. Wilkinson, J. Shen, H. Wang, J. Zhang, Journal of Power Sources 154 (2006) 202–213.
[6] S.Y. Shen, T.S. Zhao, J.B. Xu, Y.S. Li, Journal of Power Sources 195 (2010) 1001–1006.
[7] S. Song, P. Tsiakaras, Applied Catalysis B: Environmental 63 (2006) 187–193.
[8] S.C. Hall, V. Subramanian, G. Teeter, B. Rambabau, Solid State Ionics 175 (2004) 809.
[9] F. Vigier, C. Coutanceau, F. Hahn, E.M. Belgsir, C. Lamy, Journal of Electroanalytical Chemistry 563 (2004) 81–89.
[10] J.P.I. De Souza, S.L. Queiroz, K. Bergamaski, E.R. Gonzalez, F.C. Nart, Journal of Physical Chemistry B 106 (2002) 9825–9830.
[11] G.A. Camara, R.B. De Lima, T. Iwasita, Journal of Electroanalytical Chemistry 585 (2005) 128–131.

[12] L. Colmenares, H. Wang, Z. Jusys, L. Jiang, S. Yan, G.Q. Sun, R.J. Behm, Electrochimica Acta 52 (2006) 221–233.
[13] M. Nie, H.L. Tang, Z. Wei, S.P. Jiang, P.K. Shen, Electrochemistry Communications 9 (2007) 2375–2379.
[14] G. Wu, R. Swaidan, G. Cui, Journal of Power Sources 172 (2007) 180–188.
[15] P. Bommersbach, M. Mohamedi, D. Guay, Journal of the Electrochemical Society 154 (2007) B876–B882.
[16] E. Antolini, F. Colmati, E.R. Gonzalez, Electrochemistry Communications 9 (2007) 398–404.
[17] F. Colmati, E. Antolini, E.R. Gonzalez, Journal of Alloys and Compounds 456 (2008) 264–270.
[18] E. Antolini, F. Colmati, E.R. Gonzalez, Journal of Power Sources 193 (2009) 555–561.
[19] E. Lee, I.S. Park, A. Manthiram, Journal of Physical Chemistry C 114 (2010) 10634–10640.
[20] X. Zhang, D. Li, D. Dong, H. Wang, P.A. Webley, Materials Letters 64 (2010) 1169–1172.
[21] J. Datta, A. Dutta, S. Mukherjee, Journal of Physical Chemistry C 115 (2011) 15324–15334.
[22] W.C. Choi, J.D. Kim, S.I. Woo, Catalysis Today 74 (2002) 1762.
[23] G.S. Chai, J.S. Yu, Journal of Materials Chemistry 19 (2009) 6842–6848.
[24] J.F. Whitacre, T. Valdez, S.R. Narayanan, Journal of the Electrochemical Society 152 (2005) A1780–A1789.
[25] T. Iwasita, Electrochimica Acta 47 (2002) 3663.
[26] Y. Ishikawa, M.S. Liao, C.R. Cabrera, Surface Science 463 (2000) 66.
[27] M. Ammam, L.E. Prest, A.D. Pauric, E.B. Easton, Journal of the Electrochemical Society 159 (2012) B195.
[28] M. Ammam, E.B. Easton, Journal of the Electrochemical Society, Accepted March 2012, MS #JES-11–3546R1.
[29] K. Torigoe, Y. Nakajima, K. Esumi, Journal of Physical Chemistry 97 (1993) 8304–8309.
[30] L. Xiong, A.M. Kannan, A. Manthiram, Electrochemistry Communications 4 (2002) 898–903.
[31] G. Ren, H. Shi, Y. Xing, Nanotechnology 18 (2007) 385604–385610.
[32] W. Li, Q. Xin, Y. Yan, International Journal of Hydrogen Energy 35 (2010) 2530–2538.
[33] S.H. Ahn, O.J. Kwon, S.K. Kim, I. Choi, J.J. Kim, International Journal of Hydrogen Energy 35 (2010) 13309–13316.
[34] M.M. Gunter, T. Ressler, R.E. Jentoft, B. Bems, Journal of Catalysis 203 (2001) 133–149.
[35] A. Bonakdarpour, K. Stevens, G.D. Vernstrom, R. Atanasoski, A.K. Achmoeckel, M.K. Debe, J.R. Dahn, Electrochimica Acta 53 (2007) 688.
[36] L. Alonso, M. Palacios, Chemistry of Materials 14 (2002) 225.
[37] G.X. Wang, B.L. Zhang, Z.L. Yu, M.Z. Qu, Solid State Ionics 176 (2005) 1169.
[38] E. Bonetti, L. Savini, A. Deriu, G. Albanese, J. Moya, Journal of Magnetism and Magnetic Materials 262 (2003) 132.
[39] G.P. Glaspell, P.W. Jagodzinski, A. Manivannan, Journal of Physical Chemistry B 108 (2004) 9604.
[40] M. Chigane, M. Ishikawa, Journal of the Chemical Society Faraday Transactions 94 (1998) 3665.
[41] J. Pike, S.W. Chan, F. Zhang, X. Wang, J. Hanson, Applied Catalysis A: General 303 (2006) 273.
[42] R.S. Patil, M.D. Uplane, P.S. Pati, International Journal of Electrochemical Science 3 (2008) 259.
[43] K.M. Lee, D.J. Lee, H. Ahn, Materials Letters 58 (2004) 3122.
[44] O.A. Fouad, Crystal Research and Technology 41 (2006) 880.
[45] F. Montilla, E. Morallo, A.D. Battisti, A. Benedetti, H. Yamashita, J.L. Vazquez, Journal of Physical Chemistry B 108 (2004) 5044.
[46] E. Antolini, J.R.C. Salgado, E.R. Gonzalez, Journal of Power Sources 160 (2006) 957–968.
[47] Y. Shao, G. Yin, Y. Gao, Journal of Power Sources 171 (2007) 558–566.
[48] D.A. Stevens, R. Mehrotra, R.J. Sanderson, G.D. Vernstrom, R.T. Atanasoski, M.K. Debe, J.R. Dahn, Journal of the Electrochemical Society 158 (2011) B905–909.
[49] Frédéric Hasché*, Mehtap Oezaslan, Peter Strasser, ChemCatChem 3 (2011) 1805–1813.
[50] A. Kowal, M. Li, M. Shao, K. Sasaki, M.B. Vukmirovi, J. Zhang, N.S. Marinkovic, P. Liu, A.I. Frenkel, R.R. Adzic, Nature Materials 8 (2009) 325–330.